ARTICLES
PUBLISHED ONLINE: 28 OCTOBER 2012 | DOI: 10.1038/NCHEM.1477

nature chemistry

Shape-selective sieving layers on an oxide catalyst surface

Christian P. Canlas[1], Junling Lu[2], Natalie A. Ray[3], Nicolas A. Grosso-Giordano[4], Sungsik Lee[5], Jeffrey W. Elam[2], Randall E. Winans[5], Richard P. Van Duyne[1,3], Peter C. Stair[1,3,6] and Justin M. Notestein[1,4]*

New porous materials such as zeolites, metal–organic frameworks and mesostructured oxides are of immense practical utility for gas storage, separations and heterogeneous catalysis. Their extended pore structures enable selective uptake of molecules or can modify the product selectivity (regioselectivity or enantioselectivity) of catalyst sites contained within. However, diffusion within pores can be problematic for biomass and fine chemicals, and not all catalyst classes can be readily synthesized with pores of the correct dimensions. Here, we present a novel approach that adds reactant selectivity to existing, non-porous oxide catalysts by first grafting the catalyst particles with single-molecule sacrificial templates, then partially overcoating the catalyst with a second oxide through atomic layer deposition. This technique is used to create sieving layers of Al_2O_3 (thickness, 0.4–0.7 nm) with 'nanocavities' (<2 nm in diameter) on a TiO_2 photocatalyst. The additional layers result in selectivity (up to 9:1) towards less hindered reactants in otherwise unselective, competitive photocatalytic oxidations and transfer hydrogenations.

Supported and bulk oxides are ubiquitous catalysts in fuel processing, environmental or emissions control, and large-scale chemicals manufacturing, including CO hydrogenation and selective oxidation[1–5]. Non-porous, bulk oxide catalysts are often used; these can be very active and regioselective (that is, for a particular functional group), but tend not to be reactant shape-selective (that is, for a smaller molecule over a larger one). In contrast, crystalline microporous oxides such as aluminosilicate zeolites and aluminophosphates typically have pores with diameters of 0.3–1.0 nm and are important in fuels and commodities chemicals in part for their well-known ability to influence reaction pathways via reactant or transition-state shape selectivity[6]. However, not all reactions can be carried out in zeolites, and framework microporosity can impose strong diffusion limitations, excluding many larger molecules of interest to biomass utilization and fine/specialty chemicals. To combat some of these challenges, shape-selective reactions of larger molecules have been successfully carried out at pore mouths on crystallite external surfaces[7], and reactant accessibility has been improved through delamination[7,8], pillared structuring[9] or by incorporating mesoporosity[10–12]. In parallel, mesostructured oxides are available with high surfaces area and 2–50 nm pores that are able to accommodate larger reactants[13–16]. These pore structures have proven to be effective in altering the intrinsic regioselectivity or enantioselectivity of embedded active sites[17]. However, it is challenging for either class of material to select among similarly sized molecules near 1 nm, which are often too large for zeolite pores and too small for size selection in most mesostructured oxides. Molecularly imprinted oxides or films[18,19] and molecular catalysts incorporated into imprinted polymers, metal–organic frameworks (MOFs) or related materials[20] have potential for selective catalysis, but are less robust than all-oxide catalysts and may not be applicable to the same reactions.

The following work describes a novel, alternative approach that tunes the reactant selectivity of existing catalysts by introducing very thin and cavity-containing oxide sieving layers on the surfaces of larger oxide catalyst particles. These sieving layers are synthesized by the new technique of molecular-templated atomic layer deposition (ALD). Specifically, 0.3–1.5 nm ALD films are grown around surface-grafted template molecules, followed by template removal to generate oxide surface 'nanocavities' in the film. Following the size of the templates, the nanocavity dimensions are in the supermicroporous region (diameters of 1–2 nm), a region in which shape-selectivity is expected to occur for many reactants[21]. ALD makes use of self-limiting reactions between gaseous precursors and a solid surface to grow highly conformal and uniform films with subnanometre control of film thickness[22–25]. This layer-by-layer growth is ideal for many oxides, nitrides and metals and is used in the manufacture of microelectronic and optoelectronic materials[26]. We and others have recently applied it to the synthesis of supported metal catalysts[27–29] and for their partial overcoating to improve stability[30]. Templating techniques have been combined previously with oxide deposition to generate cavity structures, but to our knowledge only with much larger template dimensions (>100 nm)[31] and using methods incompatible with the high-surface-area powders typically needed to achieve useful catalytic rates. Other groups have also used thick (generally >20 nm) porous sol–gel coatings around active catalysts to alter their stability or selectivity[32,33]. In such materials, diffusion can control the observed selectivity, whereas all the materials described here are effectively non-porous particles.

---

[1]Center for Catalysis and Surface Science, Northwestern University, Evanston, Illinois 60208, USA, [2]Energy Systems Division, Argonne National Laboratory, Argonne, Illinois 60439, USA, [3]Department of Chemistry, Northwestern University, Evanston, Illinois 60208, USA, [4]Department of Chemical and Biological Engineering, Northwestern University, Evanston, Illinois, 60208 USA, [5]X-ray Science Division, Argonne National Laboratory, Argonne, Illinois 60439, USA, [6]Chemical Sciences and Engineering Sciences Division, Argonne National Laboratory, Argonne, Illinois 60439, USA. *e-mail: j-notestein@northwestern.edu

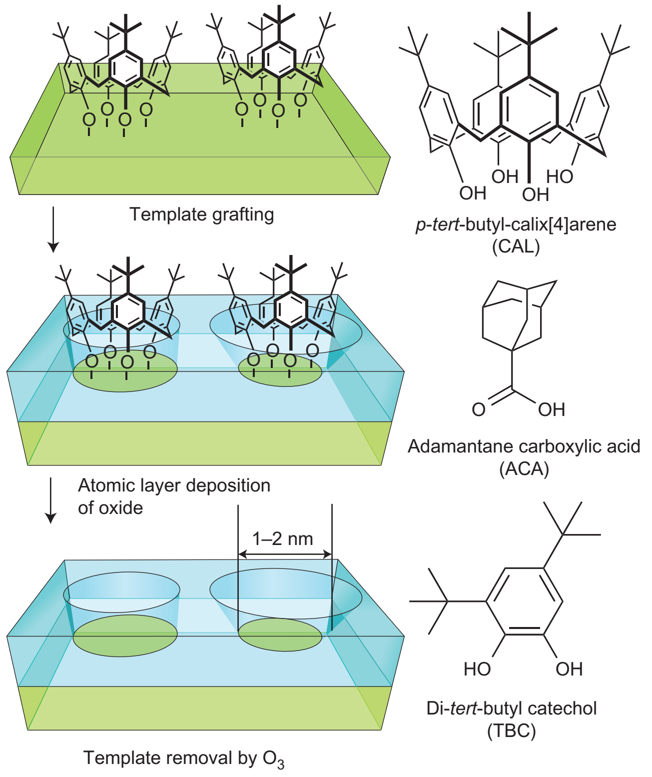

Figure 1 | Nanocavity oxides selectively allow access only to molecules able to penetrate the <2-nm-diameter supermicroporous cavities. They are synthesized by (i) depositing a template (right) onto an existing catalyst surface, (ii) using ALD to synthesize an inert oxide film <2 nm thick around, but not over, the templates, and (iii) treating the materials in O_3 to remove the templates, revealing the underlying catalyst surface.

The generalized synthesis is presented in Fig. 1. First, an appropriate template molecule is selected that will graft to the substrate but which is subsequently unreactive under ALD conditions and will remain uncovered by the ALD film. The template must also be bulky and pack poorly on the surface to allow space around the template for the ALD film. Because the templates must be grafted at submonolayer coverage, they will have a distribution of surface orientations. Consequently, relatively rigid molecules with few possible surface orientations are preferred as templates. After grafting, the ALD film is selectively deposited to a thickness less than the template height. The template is then removed to generate a nanocavity that provides selective access to the underlying surface. Based on these criteria, *p*-*tert*-butylcalix[4]arene (CAL), adamantanecarboxylic acid (ACA) and di-*tert*-butylcatechol (TBC) have been chosen as templates because they are bulky, stable and bind strongly to TiO_2 and Al_2O_3 through only one face of the molecule. In contrast, catechol is an example of a molecule not viable as a template because of its low stability and tendency to pack densely or lie flat on the surface. The nanocavity diameter and maximum depth are determined by the template dimensions, but the number of ALD cycles sets the actual cavity depth, up to the point where the template begins to be covered. For the listed templates, synthesized nanocavities are <2 nm in all dimensions, yielding <10 nm^3 cavities. The new surface morphology created by this process is demonstrated principally by transmission electron microscopy (TEM), small-angle X-ray scattering (SAXS) and quartz crystal microbalance (QCM) studies during materials synthesis. Reactant selectivity is demonstrated using alcohol photocatalytic oxidation to ketones or aldehydes and nitroaromatic photocatalytic reduction to anilines on nanocavity-modified TiO_2, which is an unselective catalyst before modification.

Results

Synthesis and characterization. ACA and CAL were grafted onto oxides from refluxing anhydrous toluene solutions, whereas TBC was deposited directly from vapour (Supplementary Methods). The chemistry for grafting phenols and carboxylic acids to Al_2O_3 and TiO_2 surfaces has been well established[34,35]. Thermogravimetric analysis (TGA) in O_2 gave CAL and ACA loadings of 25 and 60 molecules per 100 nm^2 of bare support, respectively, corresponding to ~40% of maximum packing (Supplementary Table S1, Fig. S1) The inverted conical shape of grafted calixarene dictates that even when maximally packed relative to its upper rim, smaller molecules like the ALD precursors can still access the underlying surface[36]. TBC loading on Al_2O_3 was determined by QCM to be 140 molecules per 100 nm^2 of bare support, or ~70% of a dense monolayer. After ALD and template removal, the template number density is expected to correlate approximately 1:1 with the nanocavity number density.

Template stability during ALD is required for generating nanocavities; this was verified by TGA, which revealed no change in apparent template loading after ALD (Supplementary Fig. S1), as well as by unchanged characteristic diffuse reflectance UV-visible spectra (DRUV-vis) before and after ALD (Supplementary Fig. S2). A low-energy phenol-to-TiO_2 charge transfer band appeared near 400 nm, which was unaffected by Al_2O_3 ALD, demonstrating that the template remained covalently attached to the underlying TiO_2 while being coated with Al_2O_3. This band was completely removed by final treatment in O_3. Al_2O_3 ALD on TiO_2 without a template showed no significant spectral changes, consistent with an ALD layer more transparent than the underlying oxide.

ALD of Al_2O_3 around grafted TBC was studied by *in situ* QCM (Fig. 2a, Supplementary Methods) and showed a low initial growth per cycle that slowly recovered to the steady-state value of 37 ng cm^{-2}/cycle, corresponding to 1.1 Å/cycle on bare surfaces. The recovery required ~20 ALD cycles, and the integrated missing mass was equivalent to ~880 Å^3 per cavity using the 3.0 g cm^{-3} density of ALD Al_2O_3. This value was only ~30% larger than the Connolly excluded volume of TBC of ~675 Å^3 determined using a 1.4 Å probe radius (H_2O). These data were reproducible in subsequent super-cycles and are consistent with the grafted template having suppressed Al_2O_3 ALD until sufficient layers were deposited and the template was completely overgrown after ~20 cycles or a thickness of ~2.2 nm. As a corollary, halting ALD before reaching this threshold is expected to generate accessible cavities in the ALD film once the template is removed.

SAXS was used to quantify the cavity dimensions generated in the ALD film[37] (Fig. 2, Supplementary Fig. S3). Figure 2b shows the nanocavity size distribution prepared with increasing cycles of Al_2O_3 ALD on TiO_2 with CAL templates. After 5 cycles, the scattering was consistent with cylinders 5 Å deep and averaging 10.5 Å in diameter. After 10 cycles, the diameter had not changed appreciably, but the cylinder depth increased to 11 Å, consistent with the thicker ALD layer. After 15 cycles, the apparent depth had further increased to 15 Å, and the diameter increased to accommodate the *tert*-butyl groups on the upper rim of the cone-shaped CAL.

The surface morphologies of the modified particles were observed by TEM. Figure 3a shows the relatively smooth surface for 10 cycles (1.1 nm) of amorphous Al_2O_3 deposited on single-crystal 60 nm $SrTiO_3$ cuboids (no nanocavities). Figure 3b,c shows roughness in the surface ALD layer in the presence of CAL templates. Figure 3b demonstrates that the underlying crystal face remained flat, and the surface roughness is therefore attributed to the formation of nanocavities in the ALD layer. (See also

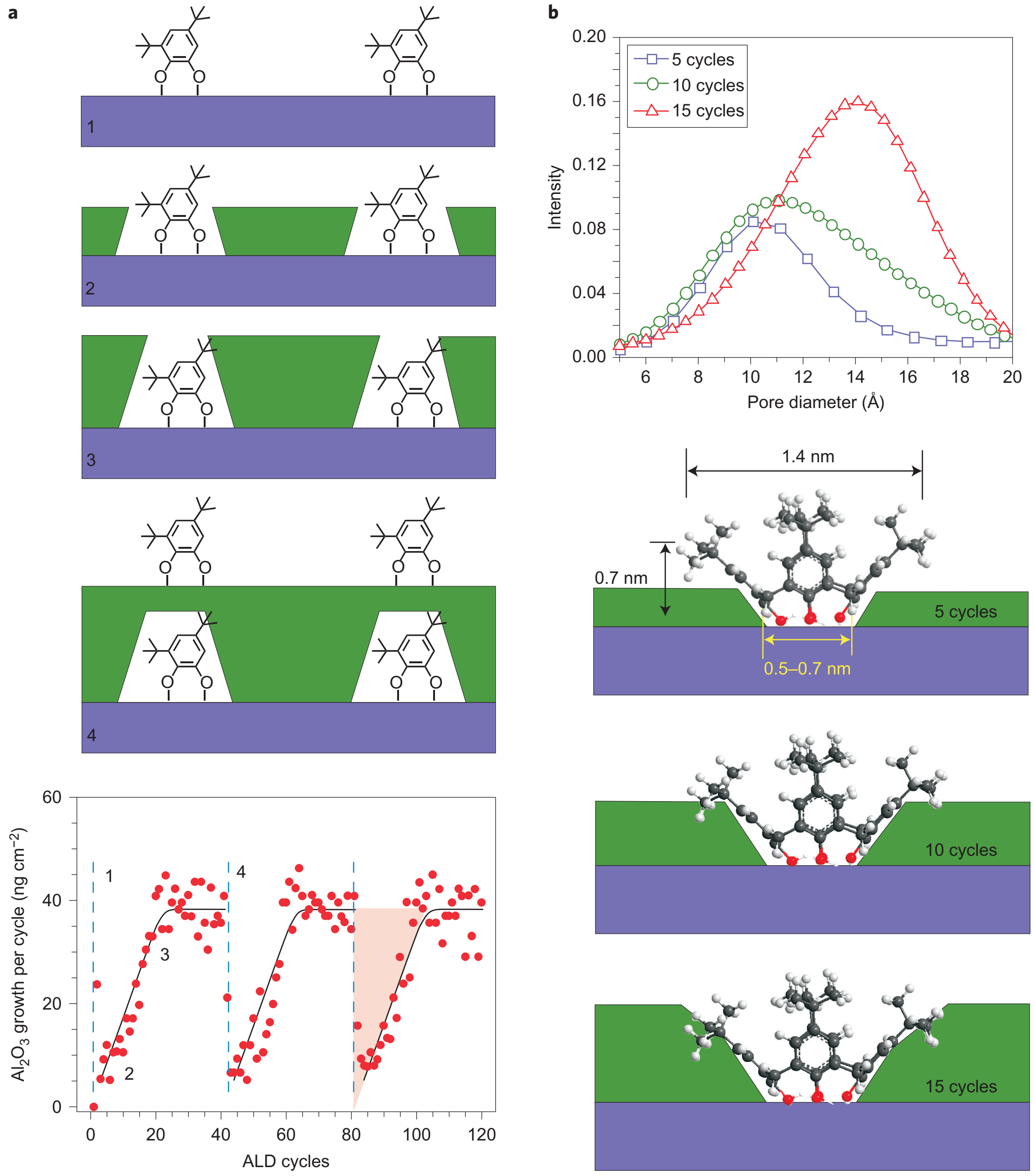

Figure 2 | Nanocavity dimensions determined by QCM and SAXS. a, Bottom: QCM measurements during three supercycles of nanocavity synthesis show adsorption of the TBC template (blue vertical lines, 1), increasing growth rates (circles, experimental data) over 20 cycles from (2) to (3) until reaching steady-state values corresponding to ~1.1 Å/cycle, and a new supercycle starting at (4). The dependence of growth rate on cycle number is consistent with this template generating ~880 $Å^3$ hemispherical or pyramidal cavities, calculated from the shaded area. **b**, SAXS data for 5, 10 and 15 cycles of Al_2O_3 ALD on CAL-TiO_2 are fit as distributions of cylindrical nanocavities with heights the same as the film thicknesses. Average diameters are 10 Å at 10 cycles and less, rising to 15 Å for 15 cycles. This pattern is consistent with the inverted conical shape of the CAL template.

Supplementary Fig. S4 for additional TEM images and magnifications of these and other materials.)

Catalytic photooxidation and photoreduction. In a series of experiments, the nanocavities were shown to control the reactant shape selectivity of nanoparticulate TiO_2 for non-aqueous UV photooxidation of alcohols using O_2 and for photoreduction of nitroaromatics with ethanol as the sacrificial reductant[38,39] (Fig. 4a). Rendered selective, TiO_2 would be an excellent, non-toxic catalyst for aerobic oxidations or transfer hydrogenations using simple alcohols, providing cost-effective and 'green' transformations[40]. Reactant-selective photooxidation by oxide catalysts has been demonstrated, but the results did not indicate size-exclusion, as will be demonstrated in the following[41–43].

Increasing cycles (1–10) of Al_2O_3 were deposited over ACA or CAL templates on Degussa Evonik TiO_2 P25, a benchmark photocatalyst. The templates were removed by O_3 treatment at 110 °C to reveal the underlying catalyst surface and selectively allow access only to molecules able to penetrate the nanocavities. Control materials were synthesized by following the same process, but in the absence of added template. The resulting materials were first tested in the competitive photooxidation of benzyl alcohol (BzOH), 2,4,6-trimethylbenzyl alcohol (TMBzOH), 2-adamantanol (AdOH) and 1-adamantane methanol (AdMeOH). Representative data are found in Fig. 4b; full data are provided in Supplementary

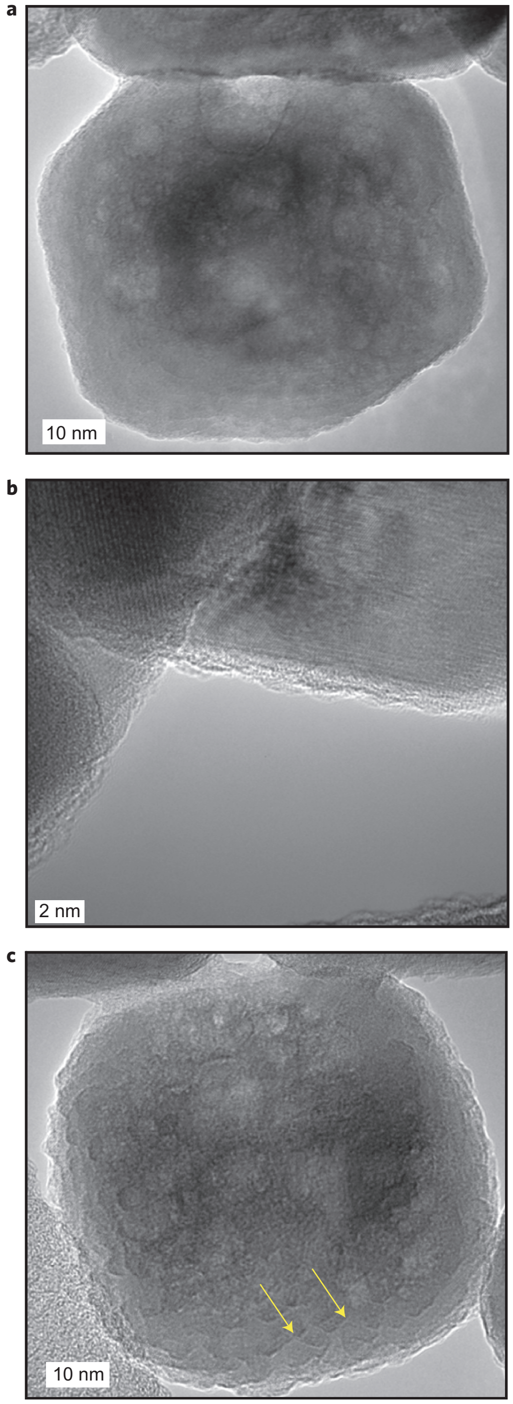

Figure 3 | TEM images show ALD-coated $SrTiO_3$ nanocuboids. **a**, Ten cycles of ALD Al_2O_3 on $SrTiO_3$ nanocuboids gives relatively smooth surfaces. **b**, High-magnification image of the roughened interface for 10 cycles of ALD Al_2O_3 on CAL-$SrTiO_3$, showing the atomically flat surface of the underlying crystal. **c**, Low-magnification image after 10 cycles of ALD Al_2O_3 on CAL-$SrTiO_3$ nanocuboids shows a much roughened surface compared to **a**. Arrows highlight several candidate nanocavities. (See Supplementary Fig. S4 for additional images and magnifications.)

Tables S2, S3, and Fig. S5. Starting from high rates on bare TiO_2, initial rates and conversions after 6 h decreased monotonically with increasing number of cycles, consistent with increasingly complete masking of the original TiO_2 catalyst surface. Absolute rates during competitive oxidation on the nanocavity catalysts were within 50% of those on the non-templated catalysts for 1–3 ALD cycles, but exceeded those on the non-templated catalysts by two- to ninefold for 5 or more cycles. Perhaps more interestingly, all absolute rates for the nanocavity catalysts levelled out beyond 5 cycles, whereas rates for the catalysts synthesized without a template dropped exponentially (Supplementary Fig. S5). Such results are consistent with the role of the template in ensuring that part of the catalytic TiO_2 surface remains uncovered at higher numbers of ALD cycles.

For both templates, oxidation rates and conversions of the secondary AdOH and of the bulky TMBzOH were more sensitive to an increasing number of ALD layers than were those of BzOH. Figure 4d plots the ratio of the initial oxidation rates for BzOH versus AdOH or TMBzOH and AdOH versus AdMeOH over CAL-templated catalysts. Over the 3 Å window in nanocavity depth from 4 to 7 cycles, rate ratios were maximized at 7.0 and 7.7 for BzOH versus AdOH and BzOH versus TMBzOH, respectively. The maxima in relative rates occurred at the number of cycles when absolute oxidation rates over the templated catalysts began to level out and greatly exceeded those on the non-templated version. This was also close to the number of cycles typically required to form pinhole-free monolayers on non-templated oxides, consistent with the notion that selective catalysis occurred at geometrically constrained sites left uncovered after template removal. ACA-templated nanocavities gave even higher maximum selectivities of 7.7 and 8.5, but with a similar trend versus number of cycles (Supplementary Table S3, Fig. S5), whereas bare TiO_2 had a relative rate of only ~1.7 for either reactant pair. Expressed differently, the nanocavities with 5 cycles of Al_2O_3 ALD gave ~87% benzaldehyde and 13% the other oxidation product when fed near-equimolar alcohol mixtures, equivalent to ~76% excess selectivity. TiO_2 gave ~56%/44% product mixtures from near-equimolar reactant mixtures, or <25% excess selectivity. Trends in peak selectivities were consistent with expectations from template and reactant dimensions. BzOH versus TMBzOH displayed higher peak selectivity than BzOH versus AdOH for both templates due to the larger reactant size difference. Similarly, the smaller ACA template gave more constrained nanocavities and higher selectivity for either reactant pair than for catalysts synthesized with the larger CAL template. In the absence of template, Al_2O_3 on TiO_2 never gave appreciable selectivities for BzOH versus AdOH, but a high rate ratio was observed for BzOH versus TMBzOH with 3 cycles of Al_2O_3. However, at 5 or more cycles, rate ratios could not be calculated accurately because of very low absolute rates (Supplementary Table S2). As additional negative controls, oxidation rates were near zero over the CAL-templated materials without previous O_3 treatment, and none of the nanocavity catalysts showed a significant preference for oxidation of AdOH versus AdMeOH for any number of ALD cycles (Fig. 4d, Supplementary Table S3), consistent with the nearly identical geometric footprints of those two reactants.

Selective photocatalytic reduction of nitrobenzene (NB) and nitroxylene (NX) with ethanol as a sacrificial reductant was also examined (Fig. 4c, Supplementary Fig. S6, Table S4). The reduction rates were similar on TiO_2 (1.2 rate ratio, 9% excess selectivity), but a rate ratio of 2.7 (46% excess selectivity) was observed on a catalyst consisting of 4 cycles of Al_2O_3 on TiO_2 using the nanocavity methodology. Most notably, no significant reaction was observed even for the less hindered NB at similar amounts of Al_2O_3 deposited without the template. The oxidation and reduction results are all consistent with a requirement for size-constrained but contiguous regions of TiO_2 at the base of the nanocavities in order to observe appreciable rates and reactant shape selectivity.

Discussion

This work has shown that indiscriminately reactive catalyst surfaces can be made reactant shape-selective through the use of partial

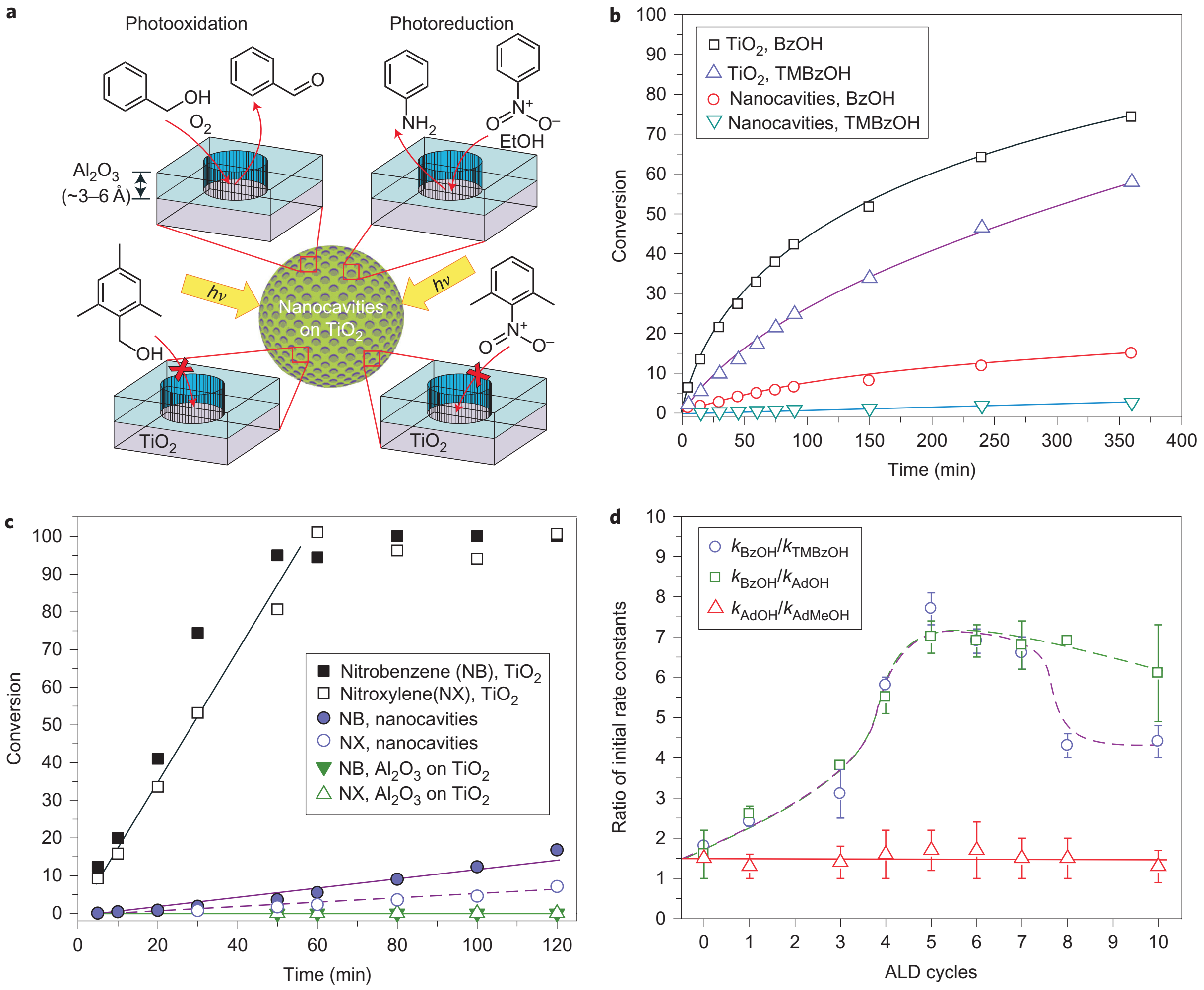

Figure 4 | Adding nanocavity-containing films adds reactant selectivity to intrinsically unselective TiO_2 photocatalysts. a, Selective photocatalytic oxidations and reductions of mixtures are carried out over CAL-templated nanocavities. **b**, Conversions of BzOH versus TMBzOH are shown over bare TiO_2 and 5 cycles of Al_2O_3 ALD on CAL-TiO_2. **c**, Conversions of NB and NX are shown over bare TiO_2, 4 cycles of Al_2O_3 on CAL-TiO_2 and 5 cycles of Al_2O_3 on TiO_2 without a template. **d**, Ratios of initial rate constants in competitive oxidations of BzOH versus TMBzOH or BzOH versus AdOH are maximized at 4–7 cycles of ALD Al_2O_3, consistent with size exclusion of larger or more hindered species once the space around the CAL template is completely filled in by the ALD process. No selectivity is observed for AdOH versus AdMeOH at any number of cycles, consistent with their identical molecular cross-sections. Full data sets and controls are provided in the Supplementary Information. In **b–d**, lines are given as guides to the eye. Panels **b** and **c** are individual experimental runs. Panel **d** gives average initial rate ratios and standard deviations of three replicates.

overcoating with an inert oxide. Because we show this using subnanometre oxide coatings, the selection mechanism cannot be based on diffusion, but instead arises from size-sieving based on the ability of the reactants to adsorb on the active catalyst surface. In this manner, analogies can be made to the selective poisoning of indiscriminate sites on catalyst surfaces. For alcohol oxidation, which requires chemisorption only at the OH group, random surface coverage by submonolayer ALD of Al_2O_3 was able to promote reactant selectivity for one reactant pair, but activity decreased rapidly with increasing number of cycles of ALD. Under these conditions, and unlike deposition over some supported metals[30], coverage of a catalytic oxide appears to be essentially complete at <8 cycles (<1 nm Al_2O_3). Although this simple procedure may find some utility for modifying catalysts, we have demonstrated here that molecular-templated ALD is more effective at maintaining higher oxidation rates and reactant selectivities at moderate numbers of ALD cycles. For reactions like nitroaromatic reduction, the nanocavity technique was essential to observe selectivity at any significant reaction rates, presumably because the reduction requires a larger adsorption footprint. Overall, these higher rates and selectivities for the templated materials are consistent with the expected role of the 1–2-nm-diameter cavities formed from one of three different template molecules and consistent with characterization by SAXS, QCM and TEM. Other templates are being explored for further control of selectivity. We note that although the smaller template did give higher maximum selectivity, this method is neither expected nor intended to give exact 'imprinting'. A distribution of template molecule configurations and surface orientations will necessarily give some distribution to the generated pore dimensions. The given nanocavity dimensions from SAXS are average sizes and, in particular, the uncovered patch of TiO_2 may be smaller than the cavity average diameter. The morphology of the nanocavity film is also expected to be affected by catalyst pretreatments, including those required for template removal. For example, high-temperature calcination may change the film structure, but does not appear to have a significant impact on catalytic selectivity.

Layered, composite catalyst particles have been known for several years as a route to control reaction selectivities, but examples are relatively rare and differ in significant ways from the catalysts described here. Catalyst particles have been overcoated with micrometre-thick, polycrystalline zeolite films[44], microporous carbon films[45] and amorphous silica layers that are tens of nanometres thick[32,33]. For the first two of these systems, the observed reaction selectivity was shown to arise from differences in diffusion through the sieving layer—a mechanism not possible for the subnanometre films in the present catalysts. Here, it has been proposed that the ALD coating modifies reactant adsorption at the catalyst sites, which has been suggested to occur in imprinted oxide films[19] and supported platinum overcoated with silicalite[46]. In general, reactant selectivity remains rare outside microporous materials, and the selectivity observed here was for molecules that differed by only a fraction of a molecular diameter, in contrast to tests of reactant selectivity in other novel, porous catalysts[20,47]. Additional investigations are under way to understand the detailed mechanism by which these nanocavities induce reactant selectivity, but regardless of the exact mechanism, reactant selectivity in the absence of an extended pore structure suggests applicability in the synthesis of larger molecules relevant to biomass or fine chemicals. Furthermore, this work has shown that the underlying oxide catalyst and ALD film composition can be chosen independently, and can include some of the most common oxides, such as Al_2O_3, TiO_2 and ZrO_2, as either support or film (Supplementary Table S1). This design flexibility potentially enables these nanocavity-containing catalysts to display a much wider range of catalyst compositions than the zeolites or related structures. We are currently applying this technique to other reaction classes and to applications beyond catalysis, including the development of new sensors, adsorbents or optoelectronic materials.

Methods

Templates were grafted from refluxing anhydrous toluene onto TiO_2, Al_2O_3 and $SrTiO_3$. $SrTiO_3$ nanocuboids were synthesized according to a previously published route[48]. In Al_2O_3 ALD, a viscous flow reactor was used with integrated QCM or powder bed at 100 °C. Cycles alternated between $Al(CH_3)_3$, purge, H_2O, and purge with N_2 carrier for 120–300–120–600 s at total 300 sccm and 1–2 torr. Note that dose and purge times are longer than typical for flat substrates. SAXS experiments were performed at the Advanced Photon Source 12ID-C undulator station with a charge coupled device detector, a q range of 0.08–2.3 $Å^{-1}$ and incident energy of 18 keV. Quantitative data analyses were performed using cylindrical form factors with a maximum entropy algorithm using the Irena package. Reactions using nanocavities were carried out in triplicate at ambient temperature, with UV illumination from a UVP Pen-Ray mercury lamp (365 nm) at a distance of ~1 inch. Under these conditions, photooxidation and photoreduction were negligible in the absence of TiO_2. ACA or CAL template was removed by O_3 treatment before reaction. Control materials had no template during ALD. Catalyst (50 mg) was suspended in solvent by magnetic stirring in 10 ml quartz test tubes. For oxidation, the solvent was acetonitrile, atmospheric O_2 was the terminal oxidant, and initial concentrations were $[BzOH]_0 = 4.83$ mM and $[AdOH]_0 = [TMBzOH]_0 = [AdMeOH]_0 = 5.00$ mM. For reduction, tubes were sealed and sparged with Ar, ethanol was the solvent/reductant, and initial concentrations were $[NB]_0 = [NX]_0 = 2.5$ mM. Reported rate ratios used first-order rate constants over the first 45–90 min. Excess selectivity was calculated as the conversion of (species 1 − species 2)/(species 1 + species 2) × 100. The only (>99%) products observed over the nanocavity catalysts were the respective aldehydes and ketones, aniline, xylidine and the condensation product between aniline and acetaldehyde. Complete details are given in the Supplementary Methods.

Received 15 June 2012; accepted 11 September 2012; published online 28 October 2012; corrected online 9 November 2012

References

1. Thomas, J. M. & Thomas, W. J. *Principle and Practice of Heterogeneous Catalysis* (VCH, 2005).
2. Satterfield, C. N. *Heterogeneous Catalysis in Industrial Practice* 2nd edn (Krieger, 1991).
3. Bartholomew, C. H. & Farrauto, R. J. *Fundamentals of Industrial Catalytic Processes* 2nd edn (Wiley, 2006).
4. Centi, G., Cavani, F. & Trifiro, F. (eds) *Selective Oxidation by Heterogeneous Catalysis* (Kluwer Academic, 2001).
5. Hoffmann, M. R., Martin, S. T., Choi, W. & Bahnemann, D. W. Environmental applications of semiconductor photocatalysis. *Chem. Rev.* **95,** 69–96 (1995).
6. Csicsery, S. M. Shape-selective catalysis in zeolites. *Zeolites* **4,** 202–213 (1984).
7. Corma, A., Fornes, V., Pergher, S. B., Maesen, T. L. M. & Buglass, J. G. Delaminated zeolite precursors as selective acidic catalysts. *Nature* **396,** 353–356 (1998).
8. Ogino, I. *et al.* Delamination of layered zeolite precursors under mild conditions: synthesis of UCB-1 via fluoride/chloride anion-promoted exfoliation. *J. Am. Chem. Soc.* **133,** 3288–3291 (2011).
9. Diddams, P. A., Thomas, J. M., Jones, W., Ballantine, J. A. & Purnell, J. H. Synthesis, characterization, and catalytic activity of beidellite-montmorillonite layered silicates and their pillared analogs. *J. Chem. Soc. Chem. Commun.* 1340–1342 (1984).
10. Chal, R., Gerardin, C., Bulut, M. & van Donk, S. Overview and industrial assessment of synthesis strategies towards zeolites with mesopores. *ChemCatChem* **3,** 67–81 (2011).
11. Valiullin, R., Kärger, J., Cho, K., Choi, M. & Ryoo, R. Dynamics of water diffusion in mesoporous zeolites. *Micropor. Mesopor. Mater.* **142,** 236–244 (2011).
12. Thomas, J. M., Hernandez-Garrido, J. C., Raja, R. & Bell, R. G. Nanoporous oxidic solids: the confluence of heterogeneous and homogeneous catalysis. *Phys. Chem. Chem. Phys.* **11,** 2799–2825 (2009).
13. Kresge, C. T., Leonowicz, M. E., Roth, W. J., Vartuli, J. C. & Beck, J. S. Ordered mesoporous molecular sieves synthesized by a liquid-crystal template mechanism. *Nature* **359,** 710–712 (1992).
14. Beck, J. S. *et al.* A new family of mesoporous molecular sieves prepared with liquid crystal templates. *J. Am. Chem. Soc.* **114,** 10834–10843 (1992).
15. Tanev, P. T. & Pinnavaia, T. J. A neutral templating route to mesoporous molecular sieves. *Science* **267,** 865–867 (1995).
16. Zhao, D. *et al.* Triblock copolymer syntheses of mesoporous silica with periodic 50 to 300 angstrom pores. *Science* **279,** 548–552 (1998).
17. Thomas, J. M. & Raja, R. Exploiting nanospace for asymmetric catalysis: confinement of immobilized, single-site chiral catalysts enhances enantioselectivity. *Acc. Chem. Res.* **41,** 708–720 (2008).
18. Katz, A. & Davis, M. E. Molecular imprinting of bulk, microporous silica. *Nature* **403,** 286–289 (2000).
19. Tada, M. & Iwasawa, Y. Design of molecular-imprinting metal-complex catalysts. *J. Mol. Catal. A* **199,** 115–137 (2003).
20. Shultz, A. M. *et al.* Selective surface and near-surface modification of a noncatenated, catalytically active metal-organic framework material based on Mn(salen) struts. *Inorg. Chem.* **50,** 3174–3176 (2011).
21. Galarneau, A., Barodawalla, A. & Pinnavala, T. J. Porous clay heterostructures formed by gallery-templated synthesis. *Nature* **374,** 529–531 (1995).
22. Cleveland, E. R., Banerjee, P., Perez, I., Lee, S. B. & Rubloff, G. W. Profile evolution for conformal atomic layer deposition over nanotopography. *ACS Nano* **4,** 4637–4644 (2010).
23. Elam, J. W., Groner, M. D. & George, S. M. Viscous flow reactor with quartz crystal microbalance for thin film growth by atomic layer deposition. *Rev. Sci. Instrum.* **73,** 2981–2987 (2002).
24. Libera, J. A., Elam, J. W. & Pellin, M. J. Conformal ZnO coatings on high surface area silica gel using atomic layer deposition. *Thin Solid Films* **516,** 6158–6166 (2008).
25. Groner, M. D., Fabreguette, F. H., Elam, J. W. & George, S. M. Low-temperature Al_2O_3 atomic layer deposition. *Chem. Mater.* **16,** 639–645 (2004).
26. Leskela, M. & Ritala, M. Atomic layer deposition chemistry: recent developments and future challenges. *Angew. Chem. Int. Ed.* **42,** 5548–5554 (2003).
27. Jiang, X., Gur, T. M., Prinz, F. B. & Bent, S. F. Atomic layer deposition (ALD) co-deposited Pt-Ru binary and Pt skin catalysts for concentrated methanol oxidation. *Chem. Mater.* **22,** 3024–3032 (2010).
28. Backman, L. B., Rautiainen, A., Lindblad, M. & Krause, A. O. I. The interaction of cobalt species with alumina on Co/Al_2O_3 catalysts prepared by atomic layer deposition. *Appl. Catal. A* **360,** 183–191 (2009).
29. Christensen, S. T. *et al.* Controlled growth of platinum nanoparticles on strontium titanate nanocubes by atomic layer deposition. *Small* **5,** 750–757 (2009).
30. Lu, J. *et al.* Coking- and sintering-resistant palladium catalysts achieved through atomic layer deposition. *Science* **335,** 1205–1208 (2012).
31. Knez, M., Nielsch, K. & Niinistoe, L. Synthesis and surface engineering of complex nanostructures by atomic layer deposition. *Adv. Mater.* **19,** 3425–3438 (2007).
32. Zhong, C. J. & Maye, M. M. Core–shell assembled nanoparticles as catalysts. *Adv. Mater.* **13,** 1507–1511 (2001).
33. Joo, S. H. *et al.* Thermally stable Pt/mesoporous silica core-shell nanocatalysts for high-temperature reactions. *Nature Mater.* **8,** 126–131 (2009).
34. Notestein, J. M., Iglesia, E. & Katz, A. Photoluminescence and charge-transfer complexes of calixarenes grafted on TiO_2 nanoparticles. *Chem. Mater.* **19,** 4998–5005 (2007).
35. O'Regan, B. & Graetzel, M. A low-cost, high-efficiency solar cell based on dye-sensitized colloidal titanium dioxide films. *Nature* **353,** 737–740 (1991).
36. De Silva, N. *et al.* A bioinspired approach for controlling accessibility in calix[4]arene-bound metal cluster catalysts. *Nature Chem.* **2,** 1062–1068 (2010).

37. Lee, S. *et al*. Selective propene epoxidation on immobilized Au_{6-10} clusters: the effect of hydrogen and water on activity and selectivity. *Angew. Chem. Int. Ed.* **48,** 1467–1471 (2009).
38. Fox, M. A. & Dulay, M. T. Heterogeneous photocatalysis. *Chem. Rev.* **93,** 341–357 (1993).
39. Zhang, M. *et al*. Oxygen atom transfer in the photocatalytic oxidation of alcohols by TiO_2: oxygen isotope studies. *Angew. Chem. Int. Ed.* **48,** 6081–6084 (2009).
40. Mallat, T. & Baiker, A. Oxidation of alcohols with molecular oxygen on solid catalysts. *Chem. Rev.* **104,** 3037–3058 (2004).
41. Shen, X. *et al*. Inorganic molecular imprinted titanium dioxide photocatalyst: synthesis, characterization and its application for efficient and selective degradation of phthalate esters. *J. Mater. Chem.* **19,** 4843–4851 (2009).
42. Ghosh-Mukerji, S., Haick, H., Schvartzman, M. & Paz, Y. Selective photocatalysis by means of molecular recognition. *J. Am. Chem. Soc.* **123,** 10776–10777 (2001).
43. Llabres i Xamena, F. X. *et al*. Enhancement of the ETS-10 titanosilicate activity in the shape-selective photocatalytic degradation of large aromatic molecules by controlled defect production. *J. Am. Chem. Soc.* **125,** 2264–2271 (2003).
44. Nishiyama, N., Miyamoto, M., Egashira, Y., & Ueyama, K. Zeolite membrane on catalyst particles for selective formation of p-xylene in the disproportionation of toluene. *Chem. Commun.* 1746–1747 (2001).
45. Foley, H. C., Lafyatis, D. S., Mariwala, R. K., Sonnichsen, G. D. & Brake, L. D. Shape selective methylamines synthesis: reaction and diffusion in a CMS–SiO_2–Al_2O_3 composite catalyst. *Chem. Eng. Sci.* **49,** 4771–4786 (1994).
46. Van der Puil, N. *et al*. Catalytic testing of TiO_2/platinum/silicalite-1 composites. *J. Chem. Soc. Faraday Trans.* **92,** 4609–4615 (1996).
47. Jones, C. W., Tsuji, K. & Davis, M. E. Organic-functionalized molecular sieves as shape-selective catalysts. *Nature* **393,** 52–54 (1998).
48. Rabuffetti, F. A. *et al*. Synthesis-dependent first-order Raman scattering in $SrTiO_3$ nanocubes at room temperature. *Chem. Mater.* **20,** 5628–5635 (2008).

Acknowledgements

This material is based on work supported as part of the Institute for Atom-efficient Chemical Transformations (IACT), an Energy Frontier Research Center funded by the US Department of Energy (DOE), Office of Science, Office of Basic Energy Science. The authors thank K. Poeppelmeier for the gift of $SrTiO_3$ nanocuboids. J.M.N. acknowledges a 3M Non-Tenured Faculty Grant, a DuPont Young Professor Grant, a Camille and Henry Dreyfus New Faculty Award and a US Department of Energy award (DE-SC0006718). S. Seifert and B. Lee are thanked for assistance with acquiring and analysing SAXS data. Use of the Advanced Photon Source, an Office of Science User Facility operated for the US DOE Office of Science by Argonne National Laboratory, was supported under contract no. DE-AC02-06CH11357. TEM was performed in the Electron Probe Instrumentation Center of NU*ANCE* (supported by NSF-NSEC, NSF-MRSEC, Keck Foundation and the State of Illinois) at Northwestern University.

Author contributions

C.P.C. grafted templates, performed TGA, UV-vis, N_2 physisorption, TEM and catalysis experiments, and wrote the paper. N.A.G.G. performed catalysis experiments. J.L. and J.W.E. performed ALD with *in situ* QCM. S.L. and R.E.W. performed SAXS. N.A.R. performed ALD with supervision by P.C.S. and R.P.v.D. J.M.N. wrote the paper, managed the collaboration and developed the initial concept.

Additional information

Supplementary information is available in the online version of the paper. Reprints and permission information is available online at http://www.nature.com/reprints. Correspondence and requests for materials should be addressed to J.M.N.

Competing financial interests

The authors declare no competing financial interests.

CORRIGENDUM

Shape-selective sieving layers on an oxide catalyst surface

Christian P. Canlas, Junling Lu, Natalie A. Ray, Nicolas A. Grosso-Giordano, Sungsik Lee, Jeffrey W. Elam, Randall E. Winans, Richard P. Van Duyne, Peter C. Stair and Justin M. Notestein

Nature Chemistry **4,** 1030–1036 (2012); published online 28 October 2012; corrected online 9 November 2012.

In the version of this Article originally published online, the affiliation for Sungsik Lee and Randall E. Winans was incorrect, it should have read 'X-ray Science Division, Argonne National Laboratory'. This has now been corrected in all versions of the Article.